Dopamine-mediated plasticity preserves excitatory connections to direct pathway striatal projection neurons and motor function in a mouse model of Parkinson's disease.

Joe C. Brague[*], Ghanshyam P. Sinha[*], David A. Henry, Daniel J. Headrick, Zane Hamdan, Bryan M. Hooks[#], and Rebecca P. Seal[#^]

Department of Neurobiology and Center for the Neural Basis of Cognition, University of Pittsburgh School of Medicine, Pittsburgh, PA 15260

* Co-first authors

Co-senior authors

^Corresponding Author: rpseal@pitt.edu `

SUMMARY

The cardinal symptoms of Parkinson's disease (PD) such as bradykinesia and akinesia are debilitating, and treatment options remain inadequate. The loss of nigrostriatal dopamine neurons in PD produces motor symptoms by shifting the balance of striatal output from the direct (go) to indirect (no-go) pathway in large part through changes in the excitatory connections and intrinsic excitabilities of the striatal projection neurons (SPNs). Here, we report using two different experimental models that a transient increase in striatal dopamine and enhanced D1 receptor activation, during 6-OHDA dopamine depletion, prevent the loss of mature spines and dendritic arbors on direct pathway projection neurons (dSPNs) and normal motor behavior for up to 5 months. The primary motor cortex and midline thalamic nuclei provide the major excitatory connections to SPNs. Using ChR2-assisted circuit mapping to measure inputs from motor cortex M1 to dorsolateral dSPNs, we observed a dramatic reduction in both experimental model mice and controls following dopamine depletion. Changes in the intrinsic excitabilities of SPNs were also similar to controls following dopamine depletion. Future work will examine thalamic connections to dSPNs. The findings reported here reveal previously unappreciated plasticity mechanisms within the basal ganglia that can be leveraged to treat the motor symptoms of PD.

KEYWORDS: Striatum, Dopamine, Plasticity, Parkinson's disease, Spiny Projection Neuron, Direct Pathway, Motor Function.

INTRODUCTION

The dorsal striatum has a critical role in voluntary movement. The major output neurons, GABAergic spiny projection neurons (SPNs) comprise >95% of striatal neurons and receive dense glutamatergic input from the cortex and thalamus and dopaminergic input from the substantia nigra pars compacta (SNpC). Direct pathway SPNs (dSPNs) express the D1 receptor and project to the substantia nigra pars reticulata (SNpR) and globus pallidus internal while the indirect pathway SPNs (iSPNs) express the D2 receptor and project to the globus pallidus external and subthalamic nucleus (Albin *et al.*, 1989; Gerfen *et al.*, 1990; Lanciego *et al.*, 2012; McGregor and Nelson, 2019; Villalba and Smith, 2010; 2018). The balance of dSPN versus iSPN output strongly influences key aspects of voluntary movement including initiation, cessation, and speed.

In Parkinson's disease (PD), the loss of SNpC dopamine input to the dorsal striatum impairs these features of voluntary movement through changes in the activity of SPNs, shifting striatal output to favor iSPNs (Smith *et al.*, 2009; Stephens *et al.*, 2005). These changes manifest as altered excitatory connectivity to SPNs and altered intrinsic excitabilities. Consistent with lost input, a reduction in mature spines and dendritic arbors of both SPN types has been observed in 6-OHDA rodent models of PD (Day *et al.*, 2006; Fieblinger *et al.*, 2014; Gagnon *et al.*, 2017; Villalba and Smith, 2018), the MPTP primate model (Smith, *et al.*, 2009; Smith and Villalba, 2008; Villalba and Smith, 2010) and postmortem brains of PD patients (Stephens *et al.*, 2005; Zaja-Milatovic, 2005). An increase in the intrinsic excitability of dSPNs has been observed consistently across rodent models, while changes in iSPNs are more variable across models. In 6-OHDA mouse models, cortical input to both dSPNs and iSPNs was shown to be similarly decreased while thalamic input from the parafasicular nucleus (PF) was increased to iSPNs and decreased to dSPNs (Parker *et al.*, 2016). In the latter case, decreasing the strength of the PF neuron connections to iSPNs after dopamine depletions restored normal motor function. Thus,

3

strategies that alter SPN extrinsic connections or intrinsic excitability, resulting in rebalanced striatal output, can be effective in alleviating PD motor deficits.

Vesicular glutamate transporter (VGLUT) 3 knockout mice were reported to exhibit normal motor behavior in the 6-OHDA depletion model of PD. Under non-depleted conditions, the mice show an increase in striatal dopamine release, locomotion, and immature spines at night (active cycle). Here we report on the mechanism that allows for normal motor behavior in these mice. First, we show that the immature spines that formed at night in VGLUT3 KO mice are exclusively on the direct pathway SPNs. Second, after dopamine depletion, we show that the density of mature spines and length of dendritic arbors are preserved also only on dSPNs. Third, the intra-striatal delivery of a D1 receptor antagonist before and during striatal dopamine depletion blocks the preservation of mature spines and arbors as well as the normal motor behavior, consistent with a requirement for increased dopamine signaling at striatal D1 receptors in the expression of these morphological behavioral phenotypes. Fourth, we show that by artificially increasing endogenous striatal dopamine using an excitatory DREADD (eDREADD) expressed in midbrain dopamine neurons of WT mice also preserves the morphology of dSPNs and the normal motor behavior following dopamine depletion similar to VGLUT3 KO mice. Fifth, the changes to the intrinsic excitability of SPNs in VGLUT3 KO and WT controls were the same. Sixth, the major excitatory input to SPNs comes from primary motor cortex layer 5 projection neurons. Here we show a profound loss of cortical input to both dSPNs and iSPNs following dopamine depletion in both VGLUT3 KO and WT mice. Thus, the preserved morphology of dSPNs in VGLUT3 KO mice following dopamine depletion does not reflect preserved connections to cortex. The basal ganglia circuit of VGLUT3 KO mice is instead protected by other mechanisms which may include thalamic connections, the other major excitatory input to the striatum. This study reveals a previously unappreciated striatal plasticity induced by the transient elevation of dopamine that preserves connections to dSPNs and can be further leveraged to treat PD patients.

RESULTS

We previously reported that striatal dopamine levels are elevated in VGLUT3 KO mice at night, and not during the day (Divito *et al,* 2015). We also reported immature spine density on a subset of SPNs is also increased at night. To determine whether the subset represents one type of SPN, we back-labeled dSPNs by injecting CTB-488 into the SNpR. One week later, mice were sacrificed at night and acute striatal slices prepared. DiI added to the acute slices labelled SPN membranes which were then analyzed for density and morphology of SPN spines on secondary dendrites. These analyses showed that only the dSPNs have increased immature spines (WT (black) vs KO (red) p<0.0001, N=3 mice per group, n=7 dendrites per group) (Figures 1A,B).

We then hypothesized that after dopamine depletion, the immature spines mature and thus maintains the normal balance of striatal output (preserves connections to dSPNs), producing normal motor behavior (Smith *et al*., 2009; Stephens *et al*., 2005). The hypothesis is based on the cocaine literature, where it has been shown that a daily administration of cocaine (which elevates dopamine) produces immature spines, which then mature following a 1–2 week period of cocaine withdrawal (in this case 6-OHDA mediated dopamine depletion) (Huang, *et al*, 2009; Lanciego *et al*, 2012; Lee, *et al*, 2013). To test whether the density of mature spines on dSPNs is maintained following dopamine depletion in VGLUT3 KO mice, we injected CTB-488 into the SNpR to back-label the dSPNs in VGLUT3 KOs and WT littermates and 6-OHDA (6 μg) into the dorsal striatum. The mice were sacrificed one week later (one cohort at night and one cohort during the day) for spine analysis. As expected, mature spines were reduced on dSPNs of WT mice at both time points (p<0.05, N=3 mice per group, n=6 dendrites per group) (Figures 1A-C). In contrast, the density of mature spines on dSPNs of VGLUT3 KO mice was not reduced at either time point (Night: N=3-4 mice per group, n=9-12 per group and Day: N=3-4 mice per group, n=6 dendrites per group) (Figure 1A and S1E). As in WT mice, immature spines on dSPNs of VGLUT3 KO mice were significantly reduced at both time points as were all types of spines on iSPNs (night: baseline vs depleted p<0.0001, day: baseline vs depleted p<0.000;

N=3 mice per group, n=7-12 dendrites per group) (Figures 1A-C). The degree of dopamine depletion was measured using tyrosine hydroxylase immunoreactivity and was similar between VGLUT3 KOs (N=12) and WT mice (N=14 mice) (Figure S1F).

We next determined the duration of the preserved motor behavior in VGLUT3 KO mice. Paw reaching in the cylinder was measured weekly until the ipsilateral paw reach was significantly greater than baseline (Figure 1D). Remarkably, VGLUT3 KO mice did not develop a significant ipsilateral paw dominance until ~5 months post-depletion (Figure 1E and Figures S1G,H).

Enhanced activation of dopamine 1 receptors is required for the preserved morphology of dSPNs and motor behavior after dopamine depletion.

Data thus far indicate that the transient increase in striatal dopamine of the VGLUT3 KO at night is likely an important component in preserving the density of mature spines on dSPNs and normal motor behavior after dopamine depletion. To test this hypothesis, we used a D1 receptor antagonist to prevent the over activation of striatal D1 receptors in VGLUT3 KO mice at night. Cannulas were bilaterally implanted in the dorsal striatum of VGLUT3 KO mice for delivery of the highly selective D1 receptor antagonist, SCH23390 or saline and in WT mice for delivery of saline (Figure 2A-C). The antagonist dosage used was determined by monitoring locomotor activity. Specifically, we identified 30 μg as the dose that reduced the locomotor activity of VGLUT3 KO mice to WT levels at night (Figure 2C). The antagonist was delivered only at the onset of the night cycle for 14 consecutive days. On day 7, all mice were injected unilaterally with 6-OHDA (6 μg) into the dorsal striatum (Figure 2A). Paw contacts in the cylinder were measured during the day both before and one week after 6-OHDA injection. Prior to depletion, all cohorts showed normal bilateral paw contacts (N=4-7 mice per cohort) (Figure 2D). After depletion, VGLUT3 KO mice infused with saline showed normal bilateral paw contacts (N=4 mice), while KO mice infused with the D1 receptor antagonist showed ipsilateral paw dominance

(ipsilateral vs contralateral p<0.0001, N=7 mice). WT mice infused with saline also showed ipsilateral paw dominance (ipsilateral vs contralateral p<0.0001, N=5 mice) (Figure 2D). The extent of dopamine depletion was similar for all cohorts (N=3-7 mice per group) (Figure 2E). These data provide strong support for the hypothesis that enhanced activation of striatal D1 receptors at night contributes to the plasticity mechanism that allows for normal motor function after dopamine depletion in VGLUT3 KO mice.

The preservation of mature spine density on dSPNs is a key feature of our model for how motor function is maintained in VGLUT3 KO mice after dopamine depletion. We therefore analyzed spine densities following this experiment. The mature spine densities on dSPNs of VGLUT3 KO control mice infused with saline were, as expected, similar in number to non-depleted VGLUT3 KO mice (N=3-4 mice per group, n=6-9 dendrites per group) (Figure 2F). in contrast, the mature spine densities on dSPNs of VGLUT3 KO mice infused with antagonist were significantly reduced (baseline vs depleted p<0.05, N=4 mice per group, n=5-9 dendrites per group). The reduction in density was similar that observed on dSPNs of WT control mice infused with saline (baseline vs depletion p<0.05; N=3 mice per group, n=6-9 dendrites per group) (Figure 2F). Spine densities on iSPNs were significantly decreased in all cohorts compared to the non-depleted controls (depleted vs non-depleted p<0.001, N=3-4 mice per group, n=6-9 dendrites per group) (Figure 2G). These data support our hypothesis that enhanced activation of D1 receptors in VGLUT3 KO mice is necessary for the preservation of mature spines on dSPNs and normal motor behavior following dopamine depletion.

A second experimental model recapitulates the dopamine-related phenotypes of VGLUT3 KO mice before and after depletion.

We hypothesize that VGLUT3 KO mice show normal motor behavior after dopamine depletion because of the increased striatal dopamine levels and enhanced activation of striatal D1 receptors which preserves the density of mature spines on dSPNs. A tight correlation between the preservation of mature spines on dSPNs and normal motor behavior was observed in all the

experiments. Nevertheless, these observations were made in mice lacking VGLUT3 globally (Seal *et al.*, 2008). These mice may have other phenotypes that are instead responsible for the preserved mature spine densities and normal motor behavior. We therefore generated a second mouse model that allows us to recapitulate exclusively the dopamine-related phenotypes of VGLUT3 KO mice (Figures 3A,B). Specifically, we expressed the excitatory Designer Receptor Exclusively Activated by Designer Drugs (eDREADD), hM3Dq into the SNpC/VTA of DAT[Cre] mice and one week later, injected CTB-488 into the SNpR to label dSPNs. Three weeks later the eDREADD ligand, clozapine-n-oxide (CNO, 0.1 mg/kg, i.p.) was injected one hour prior to the onset of the night cycle for 14 days consecutive days (Armbruster *et al.*, 2007). On Day 7, we inject 6OHDA (6 µg) into the dorsal striatum. Two control cohorts were also included in these analyses: DAT[Cre] mice expressing eDREADD, injected with saline (eDREADD+Saline, light blue) and DAT[Cre] mice expressing the mCherry reporter, injected with CNO (mCherry+CNO, dark blue) (*p<0.05, **P<0.01, ***p<0.001, ****p<0.0001; N=7-11 mice per group) (Figure 3C). The CNO dose is based on matching locomotor activity of the eDREADD mice to the level of VGLUT3 KO mice at night (Figure S3C) (Divito *et al.*, 2015).

We first tested whether this experimental paradigm preserves motor behavior, specifically contralateral forepaw reaching in the cylinder, following dopamine depletion in the eDREADD+CNO mice. Cylinder paw contacts were measured at night and during. Before depletion, all cohorts showed normal bilateral paw reaching behavior at both time points. One week after dopamine depletion, both control cohorts showed ipsilateral paw dominance at both time points (mCherry+CNO: ipsilateral vs contralateral, p<0.0001, N=12 mice; eDREADD+Saline: ipsilateral vs contralateral, p<0.0001; N=11 mice) (Figure 3E). In contrast, eDREADD+CNO mice showed no paw preference in the cylinder test at either time point (N=12-14 mice) (Figure 3E). It should be noted that CNO was not injected on the day of behavioral testing and no differences were observed in the extent of dorsal striatal dopamine depletion among the cohorts (Figure 3D).

We next examined the spine densities on SPNs of eDREADD+CNO mice and control cohorts in non-depleted and depleted conditions (Figure 3 and Figure S3). In non-depleted conditions, eDREADD+CNO and mCherry+CNO mice were injected with 0.1 mg/kg CNO and eDREADD+saline mice with saline just prior to the onset of the night cycle and the brains harvested 3 hours later. Spine analyses using acute slices showed an increase in the densities of long/thin immature spines on dSPNs of only the eDREADD+CNO mice, similar to what we observe in VGLUT3 KO (Night: eDREADD+Saline vs eDREADD+CNO, $p<0.05$; N=3-4 mice per group, n=6-9 dendrites per group) (Figure 4A and Figure S3). Remarkably, mature spine densities on dSPNs of eDREADD+CNO mice after depletion were the same as the non-depleted condition at both time points, indicating the preservation of mature spines. In contrast, and as expected, spine densities on dSPNs of control mice were significantly reduced (Night: eDREADD+Saline, baseline vs depleted, $p<0.0001$; mCherry+CNO, baseline vs depleted $p<0.001$; N=3-4 mice per group, n=6-7 dendrites per group; eDREADD+CNO, N=3 mice per group, n= 10-11 dendrites per group; Day: eDREADD+Saline, baseline vs depleted $p<0.0001$; mCherry+CNO, baseline vs depleted $p<0.01$; N=3 mice per group, n=5 dendrites per group; eDREADD+CNO, N=3 mice per group, n= 5 dendrites per group) (Figure 4A and Figure S3). Spine densities on iSPNs were significantly reduced across all cohorts both time points ($p<0.0001$, N=3 mice per group, n=5-9 dendrites per group) (Figure 4B and Figure S3).

A reduced length and complexity of dendritic arbors on both types of SPNs after dopamine depletion has been consistently reported for rodent models (Day *et al.*, 2006; Fieblinger *et al.*, 2014; Gagnon *et al.*, 2017; Villalba and Smith, 2018), the MPTP primate model (Smith, 2009; Smith and Villalba, 2008; Villalba and Smith, 2010) and postmortem brains of PD patients (Stephens *et al.*, 2005; Zaja-Milatovic, 2005). To measure dendritic arbors of SPNs, we performed Scholl analyses on striatal slices of eDREADD+CNO mice and controls before and after depletion (Figures 4C,D and Figure S2A). Prior to depletion, the degree of dendritic arbor branching by dSPNs of eDREADD+CNO mice did not differ significantly from controls (N=3 mice

per group, n=5-7 neurons per group) (Figure 4C and Figure S2A). After depletion, however, the extent of branching of dSPNs was significantly greater in eDREADD+CNO mice (*post-hoc* multiple comparisons: Black symbols compare mCherry+CNO to eDREADD+CNO mice, gray symbols compare eDREADD+Saline to eDREADD+CNO mice; *p<0.05; ●p<0.01, ■p<0.001, ▯p<0.0001; N=3 mice per group, n=5-10 neurons per group) (Figure 4D and Figure S2A). In contrast, the branching of iSPNs did not differ between eDREADD+CNO mice and control cohorts before (N=3 mice per cohort, n=5-7 neurons per cohort) or after depletion (N=3 mice per group, n=5-10 neurons per group) (Figures 4C,D and Figure S2A). In terms of the total dendritic length, dSPNs in control cohorts but not the eDREADD+CNO mice showed significantly decreased arbor length after dopamine depletion (mCherry+CNO, baseline vs depleted p<0.05; eDREADD+Saline, baseline vs depleted p<0.01; N=3-4 mice per cohort, n=5-11 neurons per group; eDREADD+CNO, N=3 mice per cohort, n= 9-11 neurons per cohort) (Figure 4E). The total dendritic lengths of iSPNs, in contrast, were significantly decreased after dopamine depletion in all cohorts (p<0.0001; N=3-4 mice per cohort, n=5-10 neurons per cohort). These data provide strong support for the hypothesis that a transient increase in striatal dopamine enhances immature spine density on dSPNs before dopamine depletion and preserves the density of mature spines and dendritic arbors on dSPNs as well as normal motor behavior after dopamine depletion.

Intrinsic electrophysiological properties of SPNs after dorsal striatal dopamine depletion.
In addition to morphological and synaptic connectivity changes, intrinsic electrophysiological properties of SPNs influence excitability and output of SPNs and thus motor deficits in models of PD (Fieblinger *et al.*, 2014). We therefore characterized the intrinsic properties of SPNs in eDREADD+CNO mice and controls, before and after dopamine depletion. Consistent with previous reports (Fieblinger *et al.*, 2014), the mean action potential (AP) frequency evoked by current injection measured for dSPNs was increased (baseline vs depletion p<0.001, N=5 mice per cohort, n=5-9 neurons per cohort), and for iSPNs was decreased (baseline vs depletion

p<0.05, N=5 mice per cohort, n=5-9 neurons per cohort). These changes in AP frequency were observed in all three cohorts (Figure S2B,C). Additionally, the resting membrane potential (Vrest) of iSPNs was significantly more negative for all cohorts (p<0.01, N=3 mice per cohort, n=5-12 neurons per cohort). Taken together with the morphological analyses, the data point to an increase in the extrinsic excitatory connections (via mature spines and preserved dendritic arbors) on dSPNs, rather than a change in intrinsic excitabilities, as the mechanism supporting normal motor function in eDREADD+CNO (and VGLUT3 KO) mice after dopamine depletion.

Loss of excitatory input from IT- and PT-type cortical projections to dSPNs and iSPNs

Motor cortex provides the main excitatory input to dorsal striatal SPNs and has been shown to be important for both motor learning and execution of movement (Currie *et al*, 2022; Park *et al*, 2022, Shinotsuka *et al*, 2023). We therefore tested whether the preserved mature spines and arbors on dSPNs observed in VGLUT3 KO (and eDREADD+CNO) mice after dopamine depletion reflect the preservation of cortical inputs to dSPNs (Figure 5). Cortical input originates from two main populations of layer 5 pyramidal neurons: IntraTelencephalic (IT-type) and Pyramidal Tract-type (PT-type) neurons (Figure 5A,B). IT-type cells project to ipsilateral and contralateral striatum and cortex, but not to other subcortical targets, while PT-type neurons project to ipsilateral striatum as well as to thalamus, subthalamic nucleus, and brainstem (Wilson, 1987; Shepherd, 2013). Well-characterized Cre driver lines were used to selectively label IT-type neurons (Tlx3_PL56-Cre) or PT-type neurons (Sim1_KJ18-Cre) (Gerfen *et al.*, 2013; Hooks *et al.*, 2018). Subcellular Channelrhodopsin-2 Assisted Circuit Mapping (sCRACM) (Petreanu *et al* 2009) was performed using the red-shifted opsin ReaChR (Lin *et al.*, 2013). AAV1 encoding Cre-dependent ReaChR-mCitrine was injected into the forelimb primary motor cortex (M1) of each Cre line at P0-P3. Acute slices were prepared at P24-158 for recording the excitatory postsynaptic currents (EPSCs) in both dSPNs and iSPNs of the dorsolateral striatum. Drd1-tomato reporter mice were used to identify dSPNs (Ade *et al.*, 2011). Tomato-negative

11

neurons that were spiny by post-hoc analysis of filled cells were considered iSPNs. Slices were stimulated with a 1 mW 473 nm laser systematically at 256 distinct points in the SPN dendritic arbor (16 x 16 squares, with 50 μm spacing) for 1 ms each in the presence of TTX and 4-AP (Figure 5C-F). Evoked current amplitudes were summed to calculate total synaptic input (in pA) as well as the area of dendritic arbor receiving cortical inputs based on the number of map points with detectable responses (~3SD > baseline).

Under non-depleted conditions, IT-type projection neurons elicited monosynaptic currents in dSPNs and iSPNs roughly equally in both VGLUT3 KO and WT controls (Figure 5G). In WT mice, iSPN input was slightly favored (∑pA=1460.7 pA ±367.3 SEM, N=22) compared to dSPN input (∑pA=780.8pA±151.4 SEM, N=28, p=0.1806). In VGLUT3 KO mice (Figure 5I), iSPN input (∑pA=1452.8 pA ±287.2 SEM, N=21) was about the same as dSPN input (∑pA=1558.0 pA ±335.8 SEM, N=25, p=0.9648). Following dopamine depletion, stimulating IT-type inputs in WT mice produced significantly less current in iSPNs (∑pA=437.9 pA ±203.3 SEM, N=9; p=0.0055 versus non-depleted mice), a 70% reduction compared to non-depleted mice. Input to dSPNs was similarly reduced (~69%) (∑pA=245.4 pA ±91.1 SEM, N=10; p=0.033 versus non-depleted mice). The reduction in EPSCs was much greater in VGLUT3 KO mice for both iSPNs (~97% loss, ∑pA=44.1 pA ±17.8 SEM, N=7; p<0.0001 versus non-depleted mice) and dSPNs (~99% loss, ∑pA=18.4 pA ±8.5 SEM, N=7; p<0.0001 versus non-depleted mice). However, the ratio of dSPN/iSPN synaptic input was roughly unaffected by dopamine depletion for both genotypes (Figure 5K).

The number of locations in the dendritic arbor receiving input (total input area) was also similar across genotypes (Figure 5H,J). For controls, dSPN input area was 16.2 pixels ±1.7 SEM, (N=28), similar to that for iSPN input (15.0 pixels ±2.3 SEM, N=22). Following dopamine depletion, this was reduced to 10.4 pixels ±0.6 SEM (N=18; p=0.0076) for dSPNs and 7.3 pixels ±1.3 SEM (N=13; p=0.0229) for iSPN. As for synaptic input strength, reduction in the area of dendritic arbor innervated was also greater for VGLUT3 KO mice. The input area of dSPNs was

reduced from 20.7 pixels ±2.2 SEM, (N=24) to 3.8 pixels ±1.9 SEM, (N=10, p<0.0001) after

dopamine loss and the iSPN input area reductions were similar (control: 20.4 pixels ±1.8 SEM,

(N=20); after dopamine loss: 5.7 pixels ±1.9 SEM, (N=12, p<0.0001). Thus, overall IT-type input

is reduced to both dSPN and iSPN following dopamine loss, and this loss is significant for both

control mice and VGLUT3 KO mice.

Results were similar for PT-type inputs (Figure 6). It is notable that overall strength of

PT-type inputs was weaker than IT-type inputs, about $1/3^{rd}$ of the strength. In primates, these

are believed to be much weaker (Pasquereau and Turner, 2010), though the PT-type

corticostriatal projection is still anatomically substantial in mouse (Hooks *et al.*, 2018). For

controls, iSPN input was again slightly favored (∑pA=476.2 pA ±126.9 SEM, N=19; Figure 6A)

compared to dSPN input (∑pA=348.7 pA ±77.1 SEM, N=25, p=0.5696). For VGLUT3 KO mice,

iSPN input (∑pA=207.3 pA ±103.9 SEM, N=7) was closer to the same as dSPN input

(∑pA=339.2 pA ±188.0 SEM, N=9, p=0.8371; Figure 6C). Testing the effects of dopamine

depletion on PT-type afferents, we observed a more severe loss of input than for IT-type inputs.

For iSPN input in WT mice, ~91% of the strength was lost (∑pA=44.7 pA ±30.2 SEM, N=9;

p=0.0006) and for dSPN input, ~82% was lost (∑pA=62.3 pA ±34.6 SEM, N=7; p=0.0071). The

PT-type loss of synaptic connectivity in VGLUT3 KO mice was even more severe, with ~1% of

the original input remaining to both iSPN (p<0.0001) and dSPN (p<0.0001). Thus, a severe loss

of excitatory input strength and dendritic area in dSPNs and iSPNs was observed for both

genotypes.

DISCUSSION

We report the induction of a striatal plasticity mechanism that supports normal contralateral paw

reaching behavior following unilateral dorsal striatal dopamine depletion. The plasticity is

induced by transiently elevating striatal dopamine at night and requires the enhanced activation

of striatal D1 receptors. It manifests as a preservation of mature spines and length and

13

complexity of dendritic arbors on dSPNs, but not iSPNs. The tight correlation between the preserved dSPN morphology and normal motor behavior in the VGLUT3 KO and eDREADD+CNO mice after dopamine depletion is consistent with a preserved balance of striatal output (i.e. direct over indirect pathway) (Smith *et al.*, 2009; Stephens *et al.*, 2005).

The motor cortex provides the major source of excitatory input to the dorsolateral striatum (Ding *et al.*, 2008) and thus a likely source of input to the mature spines that are preserved on dSPNs of eDREADD and VGLUT3 KO mice after dopamine depletion. Our connectivity data show that in control cohorts, IT-type projections provide the strongest synaptic input to dSPNs and iSPNs, roughly 3x stronger than synaptic input from PT-type neurons. Furthermore, consistent with prior experiments, IT-type inputs from motor cortex favor iSPNs over dSPNs (Wall *et al.*, 2013). After dopamine depletion, all cortical inputs measured in control cohorts were substantial lost (>70%). The reduction was notably more severe for PT-type inputs than IT-type inputs. Surprisingly, VGLUT3 KO mice also showed significant reductions in IT- and PT-type inputs to dSPNs as well as iSPNs. The preserved mature spines and arbors of dSPNs are therefore likely connected to thalamic inputs, the other major excitatory input to the dorsolateral striatum, where forelimb motor circuits are encoded. In previous studies, dopamine depletion reduced input from the parafascicular nucleus and central lateral nucleus to the dSPNs while strengthening input to iSPNs (Parker *et al.,* 2016; Tanimura *et al.*, 2022). Future work will functionally map synaptic level changes in thalamic inputs to SPNs in the experimental models.

We used a model of PD that limits dopamine depletion to the nigrostriatal pathway, thus better modeling the anatomical location of dopamine loss in human PD during the earlier stages, (Boix *et al.*, 2015). More commonly used 6-OHDA models target the median forebrain bundle, which lesions the entire midbrain dopamine system. The extent of this depletion is arguably an inaccurate representation of even late-stages of human PD (Boix *et al.*, 2015). Confirmation of our findings using rodent or monkey PD models that produce only nigrostriatal degeneration,

have neuropathology like alpha synuclein inclusions and/or mimic a slower degeneration as is seen in a subset of PD patients, will provide additional insight into the clinical utility of these findings.

Therapeutic strategies administered in the early stages of PD have the potential to delay the onset or slow the progression of motor symptoms. However, preclinical studies of PD tend to focus on late stage therapies (testing interventions administered after dopamine depletion is complete). Moreover, although dopamine replacement therapy (L-dopa) is the most effective treatment for PD symptoms, long-term use can lead to debilitating dyskinesias or lose efficacy. For these reasons, L-dopa treatment, though common, is often not administered until the late stages of the disease. Data presented here provide a strong rationale to shift administering memetics short-term at an earlier stage in the disease.

Interestingly, exercise which is employed as an adjunct treatment for PD because of its neuroprotective and restorative effects (Palasz *et al.*, 2019), elevates striatal dopamine and promotes spine enhancement within the mammalian brain (Hou *et al.*, 2017), including on dSPNs and iSPNs in PD (Toy *et al.*, 2014). The spine enhancement may be mediated though neurotrophins, which are secreted from both cortico- and nigrostriatal afferents (Baquet *et al.*, 2004; Baydyuk and Xu, 2014; Conner *et al.*, 1997). Neurotrophins play a critical role in neuronal growth, maintenance, and plasticity (Chao, 2003; Park and Poo, 2013), and have been shown to be neuroprotective in PD animal models (Nagahara and Tuszynski, 2011). Thus, mechanisms we identified here may be similarly engaged by the exercises that benefit PD patients.

Additional therapeutic strategies to induce this striatal plasticity mechanism at early stages of PD include identifying and manipulating VGLUT3$^+$ neurons that underlie the hyperdopaminergic phenotype in the KO. Striatal cholinergic interneurons express VGLUT3 and were suggested as potential candidates for the phenotype, but deletion of the transporter in these neurons had no impact on locomotor activity (Divito *et al.*, 2015). Lastly, the work may have implications for beyond motor function, for example, midbrain dopamine loss underlying

mood, sensory and cognitive symptoms commonly co-morbid in PD (Goldman *et al.*, 2018; Marras and Chaudhuri, 2016).

Author Contributions

R.P.S. conceived the study; R.P.S., J.C.B., and B.M.H designed experiments; J.C.B., G.P.S., Z.H. and D.A.H. performed the experiments, J.C.B., G.P.S., B.M.H, Z.H., D.J.H. D.A.H and R.P.S analyzed and interpreted the data; J.C.B., B.M.H. and R.P.S. wrote the paper with contributions from G.P.S.

Declaration of interests

The authors declare no competing interests.

Figure 1. Specificity of spine density phenotypes to dSPNs and duration of normal motor behavior in VGLUT3 KO mice.

(A) At baseline during the night, VGLUT3 KO mice (red solid bar) show enhanced density of immature (long/thin and stubby) spines on dSPNs compared to WT controls (black solid bar). After dopamine depletion, mature (mushroom) spine densities are significantly decreased in WT mice (blacked solid vs striped bars) but are preserved in VGLUT3 KO mice (red solid vs striped bars) across the circadian cycle. Densities of all other spine types are decreased significantly after dopamine depletion in both WT and VGLUT3 KO mice. Significant interaction by 2-way ANOVA (*genotype* x *condition*) for all spine types and time points (except stubby spines during the day; main effect $p<0.0001$).

(B) iSPN spine densities are similar at baseline in VGLUT3 KO and WT mice and all spines are decreased similarly by depletion in both genotypes. Two-way ANOVA (*genotype x condition*), no significant interaction, main effect for condition is reported.

(C) Representative images of DiI filled dSPN dendrites during the night from WT (black) and VGLUT3 KO (red) mice.

(D) Experimental paradigm measuring preserved motor behavior in VGLUT3 KO mice following dopamine depletion. CT = cylinder test. Unilateral dorsal striatal 6-OHDA (6 μg) injection. Magenta line indicates time of spine density measurement at baseline.

(E) VGLUT3 KO mice (red dots) do not show significant ipsilateral paw dominance until 20 weeks post-depletion. WT mice (gray dots) show ipsilateral dominance at 1 week. Purple and green dotted lines indicate 50% (normal) and 70% (Parkinsonian) ipsilateral paw reaches, respectively. One-way repeated measures ANOVA with Bonferroni post hoc comparison to baseline *$p<0.05$, **$p<0.01$, ***$p<0.001$, ****$p<0.0001$, ns = not significant.

Figure 2. Elevated striatal dopamine signaling through D1 receptors during dorsal striatal dopamine depletion is required for preserved d morphology and motor behavior.

(A)   Experimental paradigm for testing the role of enhanced striatal D1 receptor signaling on motor behavior and SPN morphology in a model of PD. CT=cylinder test.

(B)   Locations of bilateral cannula placement in dorsal striatum of the three cohorts. CC=corpus callosum CPu= caudate putamen, LV= lateral ventricle, AP= anterior

posterior

(C)   The dose of D1 receptor antagonist (SCH23390, 30 µg in 1 ul) delivered directly into the dorsal striatum of VGLUT3 KO mice was optimized to suppress locomotor activity to WT levels. Significant interaction by 2-way ANOVA (*cohort* x *hour*) with Bonferroni multiple comparisons.

(D)   One week after 6-OHDA injection, VGLUT3 KO mice infused with SCH23390 (purple striped bar) developed ipsilateral paw dominance similar to control WT mice infused with saline (black striped bar), while control VGLUT3 KO mice infused with saline (red striped bar) continued to show bilateral paw reaches as expected. Significant interaction by 2way ANOVA (*cohort x condition*) with Bonferroni multiple comparisons.

(E)   Percent decrease in dorsal striatal TH immunoreactivity one week after 6-OHDA injection is similar across all three animal groups, Kruskal-Wallis test.

(F)   At baseline, dSPN spine densities were similar between cohorts. After dopamine depletion, mature (mushroom) spine densities of VGLUT3 KO (D1 antagonist infused) were decreased similarly to the WT (saline infused), while control VGLUT3 KO (saline infused) showed the expected preserved mushroom spine densities. Significant interaction by 2-way ANOVA (*cohort x condition*) with Bonferroni multiple comparisons.

(G)   Baseline iSPN spine densities were similar between cohorts. After depletion, spine densities were significantly decreased across cohorts. All measurements taken during the day. No interaction by 2-way ANOVA (*cohort x condition*). Significant main effects of condition. *p<0.05, **p<0.01, ***p<0.005, ****p<0.0001, ns = not significant.

18

Figure 3. eDREADD+CNO mice show normal motor behavior following 6-OHDA mediated dorsal striatal dopamine depletion.

(A) Experimental paradigm for transiently elevating dopamine (eDREADD+CNO) in the preservation of bilateral paw reaching behavior after dorsal striatal dopamine depletion. CT_0= cylinder test at baseline, CT_1= cylinder test 1 week after dorsal striatal 6-OHDA injection. Magenta line indicates baseline spine density collection (data shown in Figure 3).

(B) Left: Illustration of Cre-dependent eDREADD (hM3Dq) viral construct and brain sites for bilateral injection of AAV8 eDREADD and CTB-Alexa488 in DAT^{Cre} mice. Middle: Confocal image eDREADD-mCherry (magenta) in midbrain dopamine neurons and CTBAlexa488 (cyan) in SNpr to back-label dSPNs. Right: Magnified confocal image. VTA- ventral tegmental area; SNpc-substantia nigra pars compacta; SNpr- substantia nigra pars reticulata. Scale bars = 500 μm.

(C) Locomotor activity is significantly elevated after CNO injection (0.1 mg/kg, i.p.) in eDREADD expressing mice (eDREADD+CNO mice, orange line) compared to control mice (dark and light blue lines). Significant interaction by 2-way ANOVA (*genotype* x *condition*). Bonferroni multiple comparison *post-hoc.*

(D) No difference between eDREADD+CNO mice (orange bar) and controls (light and dark blue bars) in percent loss of TH immunoreactivity in the dorsal striatum 1 week after 6-OHDA injection. Kruskal-Wallis test

(E) eDREADD+CNO mice (orange bars) show preserved bilateral paw reaches one week after 6-OHDA injection, while control mice show ipsilateral paw dominance (light and dark bars). No significant interaction by 2-way ANOVA (*paw x condition*) in eDREADD+CNO mice. Significant interaction and Bonferroni multiple comparisons for controls. *<0.05, **p<0.01, ***p<0.005, ****p<0.001.

19

Figure 4. eDREADD+CNO mice recapitulate the morphological changes observed in SPNs of VGLUT3 KO mice after dorsal striatal dopamine depletion.

(A)　At baseline, immature (long/thin) d spine density in eDREADD+CNO mice (orange solid bars) is enhanced compared to control eDREADD+saline (light blue solid bars) only during the night. After depletion, mature (mushroom) spine density is preserved in eDREADD+CNO mice (orange solid vs striped bars) but not in control (light blue solid vs striped bars) across the circadian cycle. mCherry+CNO control located in Extended data S3 for illustrative purposes. Significant interaction by 2-way ANOVA (*cohort* x *condition*) mushroom and long/thin spines. Bonferroni multiple comparisons. No interaction stubby and long/thin spines during the day. Significant main effect for condition.

(B)　Depletion decreased iSPN spine densities to the same extent in eDREADD+CNO mice (orange bar) and control (light and dark blue bars). No interaction by 2-way ANOVA (*cohort x condition*). Significant main effect for condition.

(C)　Number of intersections by dSPN and iSPN dendrites in dorsal striatum is similar across cohorts at baseline (left). No interaction by 2-way ANOVA (*cohort x intersection*). After dopamine depletion, intersections by dSPNs in eDREADD+CNO mice (light orange dots, right) are significantly enhanced compared to control cohorts (light purple and light blue dots). Significant interaction by 2-way ANOVA (*cohort x intersection*). Bonferroni multiple comparisons. Black symbols compare eDREADD+CNO mice to mCherry+CNO controls, grey symbols compare eDREADD+CNO mice to eDREADD+Saline controls. *p<0.05; ●p<0.01, ■p<0.001, ▨p<0.0001.

(D)　eDREADD+CNO mice (dark and light orange dots), but not controls (dark and light purple and blue dots) show preserved total dendritic length of dSPNs after dopamine depletion. Significant interaction by 2-way ANOVA (*cohort x condition*). Bonferroni multiple comparisons. Total dendritic length of iSPNs is decreased significantly within all cohorts after depletion. No interaction by 2-way ANOVA (*animal group x condition*). *p<0.05, **p<0.01, ***p<0.005, ****p<0.001, ns = not significant.

20

Figure 5. Quantification of Cell Type-Specific Corticostriatal Connection Strength

(A) Layer 5 IT-type (gray) and PT-type (black) neurons project to dSPN (blue) and iSPN (red) in striatum. Thalamus (green) also excites these targets.

(B) Cre-driver mouse lines label IT-type neurons (top, PL56-Cre) and PT-type neurons (bottom, KJ18-Cre) with AAV-DIO-EGFP. Image shows cell bodies in forelimb M1, with pia and white matter (WM) marked for reference. The laminar distribution of labeled neurons in these mouse lines is shown in the center. At right, example reconstructed axons of a single IT-type neuron (blue) and a single PT-type neuron (gold) are shown from above, with targets in cortex (ctx), striatum (str), thalamus (thal), and superior colliculus (SC) shown.

(C) Stereotaxic AAV injection of Cre-dependent opsin makes IT-type (green; or PT-type, not shown) axons excitable for recording input to dSPN (transgenically labeled with Drd1a-tdTomato) or in neighboring iSPN cells. Experiments test whether input is strong or weak and clustered or diffuse.

(D) 60x fluorescence image of tdTomato+ dSPN in a PL56-Cre+, Drd1a-tdTomato+ striatal brain slice.

(E) 4x brightfield image of coronal brain slice. dSPN soma (center, red circle) shown with teal points for input mapping with sCRACM. 16x16 array of points are spaced at 50 mm.

(F) Responses to 1 ms, 1 mW 470 nm laser stimuli displayed in relative location in the dendritic arbor. Non-responsive points are flat. Inset shows mean responses at each point aligned (mean of 2-5 sweeps). Total EPSC amplitude and number of input points is quantified.

(G) Total EPSC amplitude on a log scale to dSPN and iSPN from IT-type neurons in naive conditions and following 6-OHDA depletion.

(H) Dendritic input area to dSPN and iSPN from IT-type neurons, plotted as for EPSC strength. (I,J) Total EPSC amplitude on a log scale and dendritic input area to dSPN and iSPN from IT-type neurons in naive conditions and following 6-OHDA depletion for VGLUT3 KO mice.

21

(I)   (K) dSPN/iSPN input ratio for summed EPSC amplitude. Data are compared by Mann-Whitney. *, p<0.05; **, p<0.01, ***, p<0.001.

Figure 6. Quantification of Cell Type-Specific Corticostriatal Connection Strength from PT-type corticostriatal inputs

(A)   Total EPSC amplitude on a log scale to dSPN and iSPN from PT-type neurons in naive conditions and following 6-OHDA depletion.

(B)   Dendritic input area to dSPN and iSPN from PT-type neurons, plotted as for EPSC strength.

(C)   Total EPSC amplitude on a log scale and dendritic input area to dSPN and iSPN from PT-type neurons in non-depleted conditions and following 6-OHDA depletion for VGLUT3 KO mice.

(D)   dSPN/iSPN input ratio for summed EPSC amplitude. Data are compared by Mann-Whitney. *, p<0.05; **, p<0.01, ***, p<0.001.

STAR METHODS

LEAD CONTACT AND RESOURCE AVAILABILITY

Further information and requests for reagents and resources should be directed and will be fulfilled by Rebecca Seal (rpseal@pitt.edu). Raw data obtained for this study are available from the lead contact upon request. Code generated for data analysis is available upon request. Any additional information required to reanalyze the data reported here is available from the lead contact upon request.

Experimental Animal and subject details

Animals were housed in micro-isolator cages on a reverse 12h night/day cycle (10 A.M. lights off, 10 P.M. lights on). All animals had *ad libitum* access to food and water and were treated in compliance with Institutional Animal Care and Use Committee for the University of Pittsburgh. All efforts were made to minimize the number of animals used and to avoid pain and discomfort. In each experiment, approximately equal numbers of males and females were used. *Slc17a8*$^{-/-}$ mice (also referred to as VGLUT3$^{-/-}$ or VGLUT3 KO mice) were backcrossed at least 10 generations to C57BL/6. DAT^{cre} (RRID: IMSR_JAX:020080) and D1^{dt} (RRID: IMSR_JAX:016204) were obtained from Jackson laboratories. For eDREADD experiments, DAT^{cre} mice were used. For electrophysiological eDREADD experiments, DAT^{cre} and D1^{dt} mice were crossed to obtain DAT^{cre}; D1^{dt} mice. When testing the duration of normal motor behavior in VGLUT3 KO mice following DA depletion, experiments began between the age of 3-5 months and ended at 8-10 months. For all remaining experiments, mice were 3-6 months in age.

Animal Groups and Experimental Approach

Experiment 1: SPN spine morphology in a dopamine depleted state. VGLUT3 KO and WT mice were used. Experiment 2: Effects of transient elevated dopamine on motor behavior, spine dynamics, and electrophysiology of SPNs in normal and dopamine depleted states. DAT^{cre}; D1^{dt} mice were used for electrophysiology experiments and DAT^{cre} mice were used for the remaining experiments. Mice in these experiments were randomly divided into three cohorts: 1) mCherry+CNO, 2) eDREADD+Saline, or 3) eDREADD+CNO. At 3 months of age, mice were injected with the eDREADD or mCherry virus bilaterally into the SNpc (details below). At least three weeks following viral injection, eDREADD and mCherry animals were given either saline or CNO one hour before the lights were out (Zeitgerber = 12 for lights out) for 5 days. These animals then underwent baseline behavioral testing. The injections continued daily for 7 days following dopamine depletion via 6-OHDA. Animals were assessed behaviorally, one-week

23

following depletion. Animals were euthanized during the day and at night and assessed for spine and dendrite morphology and electrophysiology.

Behavior

Light conditions and temperature were kept at ambient levels (~32 lux, 75°C). For homecage locomotor activity, mice were placed in rat micro-isolator cages inside a photobeam monitoring system (Kinder Scientific) for 72 hours with food and water *ad libitum*. For the *cylinder test*, mice were placed in a clear glass cylinder ~8 cm in diameter with a clear acrylic sheet on top. The video camera was placed overhead and recorded one 5-minute video per animal per condition. The number of full weight-bearing forepaw contacts (identified as the majority of the forepaw coming in contact with the cylinder) against the cylinder wall was recorded and expressed as total percentage of contacts. Paw dominance is equal to or greater than 70% ipsilateral paw contacts in the cylinder test. Animals were tested 3-4 hours before and after the start of the night cycle on separate days. Videos with less than 7 total rears were excluded from analysis. All videos were scored by two trained observers unaware of the treatment groups. Their scores were compiled and averaged together.

Stereotaxic Surgery

All surgical procedures were performed using aseptic technique. Mice were anesthetized with a 3% induction/1-3% maintenance of isoflurane/100% oxygen mixture. Specific details of surgery can be found in Divito *et al* 2015. Briefly, for eDREADD injections, mice were either given 1 μL of AAV8-hSyn-DIO-hM4d(Gi)-mCherry (**RRID**: Addgene_44362) or AAV8-hSyn-DIO-mCherry (**RRID**: Addgene_50459) bilaterally into the SNpC (in mm) 3.29 AP, ±1.30 ML, and -4.40 DV. For 6-hydroxydopamine hydrochloride (6-OHDA) injections, mice were given unilateral partial dorsal striatal lesions to assess Parkinsonian motor behavior. Stereotaxic coordinates used for the unilateral injection of 6-OHDA (6 μg, Sigma) or saline were (in mm) +0.85 AP, -1.75 ML, and -

2.75 DV. Injections were administered at 0.25µL/min with three-minute incubation periods following needle placement and solution injection. Immediately following surgery, mice were sutured and administered ketoprofen (Ketofen 5 mg/kg, Zoetis) and allowed to recover for one week.

Mice also received IP injections of 0.9% saline (0.5mL) 1-2x daily for 6 days after surgery. Mouse weight was monitored and any that lost >20% of their presurgical weight were excluded. No animals were lost or euthanized after surgery due to surgical complications. 6-OHDA injected animals with less than 70% decrease in tyrosine hydroxylase (TH) staining across the rostral-caudal extent of the dorsal striatum were excluded from analysis. Baseline behavior tests were performed at least three-weeks following eDREADD injections and post-depleted behaviors were assessed one-week following 6-OHDA depletion. Brains were either harvested for spine analysis or electrophysiology (see below).

For electrophysiology experiments mapping input from specific cortical cell types to striatum, mice from two GENSAT BAC Cre-recombinase driver lines (Tlx3_PL56 for IT-type neurons and Sim1_KJ18 for PT-type neurons) were used (Gerfen *et al.*, 2013). To maximize time for expression, offspring were injected perinatally at postnatal day (P) 0-3 with a Cre-dependent AAV expressing the red-shifted opsin ReaChR (AAV-flex-ReaChR-citrine, Addgene 50955; Lin JY, Tsien R, *et al.*, 2013 Nat Neurosci). Pups were cryo-anesthetized with ice for 6-8 minutes and placed in a clay mold stored in a -20 C freezer between uses. The mold aided in positioning pups during injections while maintaining low temperature. Because bregma is not visible at this age, the confluence of the sinuses, approximately corresponding to lambda, was used for alignment. Because the borosilicate glass used for the injection can pass through the skin and skull at this age, and incision is not necessary. The injection was made at 1800 µm anterior and 1100 µm lateral at two depths measured from the skin (850 µm and 650 µm). 100 nL was injected at each site.

Cannulation Surgery and Infusion Procedures

Mice were anesthetized with a 3% induction/1-3% maintenance of isoflurane/100% oxygen mixture. An incision was made in the midline of the skull and 2 small burr holes were drilled through the skull at stereotaxic coordinates +0.85 AP and -/+1.75 ML. Low profile 26 Ga, 1.75 mm guide cannulas (Plastics One 42593), containing a 33 Ga, 2.75mm internal dummy cannula (Plastics One 42597) were implanted into these coordinates at a depth of -2.75 DV and secured with GC FujiCem 2 glass ionomer cement (Fisher, 5081153). The wound was sutured closed if any remaining bone or musculature were exposed. Ketoprofen (Ketofen 5 mg/kg, Zoetis) was administered immediately following surgery and the mice allowed to recover for one week. Mice also received IP injections of 0.9% saline (0.5mL) 1-2x daily for 6 days after surgery. Mice were singly housed following surgical procedures to avoid accidental loss of cannulas. Mouse weight was monitored and any that lost >20% of their presurgical weight were excluded. To infuse saline or D1R antagonist (Tocris, SCH-23390) bilaterally into the striatum, mice were first pinned down with a cloth, had their internal dummy cannulas removed, and placed the internal infusion cannula (Plastics One, 42595) into the right and left guide cannula. 1µL of saline or D1R antagonist (SCH-23390, TOCRIS) were infused at a rate of 0.25µl/min into each hemisphere while the mice moved freely. Three minutes following infusion, the mouse was again pinned down, the infusion cannulas removed, the internal dummy cannula inserted, and the mouse was placed back into the home cage. Prior to behavioral testing, all mice were acclimated to infusion procedures with 3 days of saline injections.

Dil labeling and Immunohistochemistry

To analyze spine morphology, mice were euthanized with an overdose of ketamine/xylazine and intracardially perfused with 25 mL PBS (in mm): 7.95 NaCl, 0.20 KCl, 1.425 Na_2HPO_4, 0.27 KH_2PO_4, followed by 50mL of cold PBS with 2.5% paraformaldehyde in PBS (para). Brains were dissected and postfixed for one hour in 2.5% para. Brains were then sectioned at 100µm on a

vibratome (LEICA VT1000S) and every other section was wet mounted onto a slide. Small DiI (Thermofisher, D3911) crystals were then placed on the dorsal striatum via glass micropipette. Sections were incubated in PBS at 4°C for two days and subsequently fixed with 4% para for one hour at room temperature. The slides were then coverslipped and stored at 4°C until imaged on a confocal. The remaining slices were fixed in 4% para before being stained for TH immunoreactivity. Slices were washed (3x5 minutes) in PBS and incubated in 1:1000 Rabbit α-tyrosine hydroxylase (RRID: AB_390204) containing 0.4%Triton X-100 and 5% normal donkey serum in PBS for 48 hours at room temperature. After washing, these slices were then incubated in 1:500 Alexa Fluor 488 conjugated donkey α-rabbit (RRID:

AB_2313584) containing 0.4%Triton X-100 for two hours at room temperature and then mounted with DAPI Fluromount-G (southern Biotech, 0100-20). For electrophysiology experiments, a 1:500 Alexa Fluor 647 streptavidin (RRID: AB_2341101) was added to the secondary solution for neurobiotin labeling. Labeled neurons were imaged on a confocal at 40x with NIS-elements (RRID: SCR_014329) software, then traced and analyzed for Sholl intersections using Simple Neurite Tracer in Fiji-ImageJ (RRID: SCR_002285) software.

Electrophysiology

Coronal sections (300 μm thickness) were prepared from brains of mice 3-6 months in age of both sexes and euthanized before the onset of the night cycle (10 am). Slices were cut in ice-cold, carbogenated, N-methyl-D-glucamine-HEPES solution containing the following (in mM): 93 N-methyl-D-glucamine, 2.5 KCl, 1.2 NaH_2PO_4, 30 $NaHCO_3$, 20 HEPES, 25 glucose,10 $MgSO_4$, 0.5 $CaCl_2$, 5 sodium ascorbate, 2 thiourea, and 3 sodium pyruvate, pH 7.3. Slices were allowed to recover for 15 minutes at 33°C in this solution before being held at room temperature for 1 hour in carbogenated artificial cerebral spinal fluid (ACSF) as follows (in mM): 125 NaCl, 26 $NaHCO_3$, 1.25 NaH_2PO_4, 2.5 KCl, 12.5 glucose, 1 $MgCl_2$, and 2 $CaCl_2$. Recordings were made at 33°C using oxygenated ASCF. Whole-cell patch-clamp recordings were performed using

borosilicate pipettes (46 MΩ resistance) filled with an internal solution containing either potassium methylsulfonate or potassium gluconate (in mM): 130 KMeSO$_3$, 10 NaCl, 2 MgCl$_2$, 0.16 CaCl$_2$, 0.5 EGTA, 10 HEPES, 2 Mg-ATP, and 0.3 Na$_2$-GTP with 0.2% Neurobiotin (RRID: AB_2336606), pH 7.3, or 128 potassium gluconate, 4 MgCl$_2$, 10 HEPES, 1 EGTA, 4 Na$_2$-ATP, 0.4 Na$_2$-GTP, 10 sodium phosphocreatine, and 3 sodium L-ascorbate, pH 7.27. Cells in which series resistance changed >20% over the course of the recording were excluded from analysis. Data were collected and analyzed using pClamp-10 (RRID: SCR_011323) software. For sCRACM laser scanning photostimulation experiments, data were acquired at 10 kHz using an Axopatch 700B (Molecular Devices) and Wavesurfer software (https://wavesurfer.janelia.org/) on a custom-built laser scanning photostimulation microscope (Shepherd *et al.*, 2003). During sCRACM mapping, neurons were held at –70 mV. A blue laser (473 nm, CrystaLaser) was controlled via scan mirrors (Cambridge Technology). Light pulses were controlled with a shutter (4 ms open time) in series with an acousto-optic modulator (1 ms pulse, QuantaTech) to deliver ~0.5–2 mW at the specimen plane through a low-power objective (UPlanApo 4✗, 0.16 NA, Olympus). Laser power was constant during a given day. Sweeps consisted of 100 ms baseline and 300 ms following onset of the stimulus. The map grid (16 ✗ 16 sites at 50 µm spacing) was centered horizontally over the soma of the recorded neuron and covered the entire SPN dendritic arbor. Maps were repeated 2–4 times and averaged across trials. LED stimuli for short-term plasticity were delivered using flashes of a 470 nm LED (Cairn). Sweeps were interleaved and repeated 4–6 times per stimulus frequency.

Statistics

The Kruskal-Wallis Test was used to analyze the percent decrease in TH immunoreactivity in the dorsal striatum. A mixed effect model with repeated measures was used to analyze depleted animals over the course of 20 weeks. For the remaining analyses, we used a two-way ANOVA, repeated measures analysis (*condition vs genotype or condition vs mouse type*). If no significant interaction was found, we reported the main effect. If a significant interaction was found, we

used *post-hoc* comparisons with a Bonferroni correction. All data were measured for normality against a Gaussian distribution, using both Shapiro-Wilk and Kolmogorov-Smirnov tests (alpha=0.05). Significance was determined at $p<0.05$. All data are represented as mean ± SEM. All analyses were performed in GraphPad Prism 8 (RRID**:** SCR_002798) software. *$p<0.05$, **$p<0.01$, ***$p<0.001$, ****$p<0.0001$

SUPPLEMENTAL INFORMATION

Document S1. Figures S1-S3.

REFERENCES

Ade, K.K., Wan, Y., Chen, M., Gloss, B., and Calakos, N. (2011). An Improved BAC Transgenic Fluorescent Reporter Line for Sensitive and Specific Identification of Striatonigral Medium Spiny Neurons. Front Syst Neurosci 5, 32. 10.3389/fnsys.2011.00032

Albin, R.L., Young, A.B., and Penney, J.B. (1989). The functional anatomy of basal ganglia disorders. *12*, 336-375.

Armbruster, B.N., Li, X., Pausch, M.H., Herlitze, S., and Roth, B.L. (2007). Evolving the lock to fit the key to create a family of G protein -coupled receptors potently activated by an inert ligand. PNAS *104*, 5163-5168.

Baquet, Z.C., Gorski, J.A., and Jones, K.R. (2004). Early striatal dendrite deficits followed by neuron loss with advanced age in the absence of anterograde cortical brain-derived neurotrophic factor. J Neurosci *24*, 4250-4258. 10.1523/JNEUROSCI.3920-03.2004.

Baydyuk, M., and Xu, B. (2014). BDNF signaling and survival of striatal neurons. Front Cell Neurosci *8*, 254. 10.3389/fncel.2014.00254.

Boix, J., Padel, T., and Paul, G. (2015). A partial lesion model of Parkinson's disease in mice--characterization of a 6-OHDA-induced medial forebrain bundle lesion. Behav Brain Res *284*, 196-206. 10.1016/j.bbr.2015.01.053.

Chao, M.V. (2003). Neurotrophins and their receptors: a convergence point for many signalling pathways. Nat Rev Neurosci *4*, 299-309. 10.1038/nrn1078.

Conner, J.M., Lauterborn, J.C., Yan, Q., Gall, C.M., and Varon, S. (1997). Distribution of Brain-Derived Neurotrophic Factor (BDNF) Protein and mRNA in the Normal Adult Rat CNS: Evidence for Anterograde Axonal Transport. J Neurosci *17*, 2295-2313.

Currie, S.P., Ammer, J.J., Premchand, B., Dacre, J., Wu, Y., Eleftheriou, C., Colligan, M., Clarke, T., Mitchell, L., Faisal, A.A., Hennig, M.H., and Duguid, I. (2022). Movement-specific signaling is differentially distributed across motor cortex layer 5 projection neuron classes. Cell Rep. *39*, 110801. 10.1016/j.celrep.2022.110801.

Day, M., Wang, Z., Ding, J., An, X., Ingham, C.A., Shering, A.F., Wokosin, D., Ilijic, E., Sun, Z., Sampson, A.R., *et al*. (2006). Selective elimination of glutamatergic synapses on striatopallidal neurons in Parkinson disease models. Nat Neurosci *9*, 251-259. 10.1038/nn1632.

Ding, J., Peterson, J.D., and Surmeier, D.J. (2008). Corticostriatal and thalamostriatal synapses have distinctive properties. J Neurosci *28*, 6483-6492. 10.1523/JNEUROSCI.0435-08.2008.

Divito, C.B., Steece-Collier, K., Case, D.T., Williams, S.P., Stancati, J.A., Zhi, L., Rubio, M.E., Sortwell, C.E., Collier, T.J., Sulzer, D., *et al*. (2015). Loss of VGLUT3 Produces Circadian-Dependent Hyperdopaminergia and Ameliorates Motor Dysfunction and lDopa-Mediated Dyskinesias in a Model of Parkinson's Disease. J Neurosci *35*, 1498314999. 10.1523/JNEUROSCI.2124-15.2015.

Fieblinger, T., Graves, S.M., Sebel, L.E., Alcacer, C., Plotkin, J.L., Gertler, T.S., Chan, C.S., Heiman, M., Greengard, P., Cenci, M.A., and Surmeier, D.J. (2014). Cell typespecific plasticity of striatal projection neurons in parkinsonism and L-DOPA-induced dyskinesia. Nat Commun *5*, 5316. 10.1038/ncomms6316.

Gagnon, D., Petryszyn, S., Sanchez, M.G., Bories, C., Beaulieu, J.M., De Koninck, Y., Parent, A., and Parent, M. (2017). Striatal Neurons Expressing D1 and D2 Receptors are Morphologically Distinct and Differently Affected by Dopamine Denervation in Mice. Sci Rep *7*, 41432. 10.1038/srep41432.

Gerfen, C.R., Engber, T.M., Mahan, L.C., Susel, Z., Chase, T.N., Monsma, F.J., and Sibley, D.R. (1990). D1 and D2 dopamine receptor-regulated gene expression of striatonigral and striatopallidal neurons. Science *250*, 1429-32. 10.1126/science.2147780

Gerfen, C.R., Paletzki, R., and Heintz, N. (2013). GENSAT BAC cre-recombinase driver lines to study the functional organization of cerebral cortical and basal ganglia circuits. Neuron *80*, 1368-1383. 10.1016/j.neuron.2013.10.016

Goldman, J.G., Vernaleo, B.A., Camicioli, R., Dahodwala, N., Dobkin, R.D., Ellis, T., Galvin, J.E., Marras, C., Edwards, J., Fields, J., *et al*. (2018). Cognitive impairment in Parkinson's disease: a report from a multidisciplinary symposium on unmet needs and future directions to maintain cognitive health. NPJ Parkinsons Dis *4*, 19. 10.1038/s41531018-0055-3.

Hooks, B. M., Papale, A. E., Paletzki, R. F., Feroze, M. W., Eastwood, B. S., Couey, J. J., Winnubst, J., Chandrashekar J., and Gerfen, C. R. (2018). Topographic precision in sensory and motor corticostriatal projections varies across cell type and cortical area. Nat Comms *9*. 3549. https://doi.org/10.1038/s41467-018-05780-7

Hou, L., Chen, W., Liu, X., Qiao, D., and Zhou, F.M. (2017). Exercise-Induced Neuroprotection of the Nigrostriatal Dopamine System in Parkinson's Disease. Front Aging Neurosci *9*, 358. 10.3389/fnagi.2017.00358.

Huang, Y.H., Lin, Y., Mu, P., Lee, B.R., Brown, T.E., Wayman, G., Marie, H., Liu, W., Yan, Z., Sorg, B.A., *et al.* (2009). In vivo cocaine experience generates silent synapses. Neuron *63*, 40-47. 10.1016/j.neuron.2009.06.007.

Lanciego, J.L., Luquin, N., and Obeso, J.A. (2012). Functional neuroanatomy of the basal ganglia. Cold Spring Harb Perspect Med *2*, a009621. 10.1101/cshperspect.a009621. Lee, B.R., and Dong, Y. (2011). Cocaine-induced metaplasticity in the nucleus accumbens: silent synapse and beyond. Neuropharmacology *61*, 1060-1069. 10.1016/j.neuropharm.2010.12.033.

Lee, B.R., Ma, Y.Y., Huang, Y.H., Wang, X., Otaka, M., Ishikawa, M., Neumann, P.A., Graziane, N.M., Brown, T.E., Suska, A., *et al.* (2013). Maturation of silent synapses in amygdala-accumbens projection contributes to incubation of cocaine craving. Nat Neurosci *16*, 1644-1651. 10.1038/nn.3533.

Lin, J.Y., Knutsen, P.M., Muller, A., Kleinfeld, D., and Tsien, R.Y. (2013) ReaChR: a red-shifted variant of channelrhodopsin enables deep transcranial optogenetic excitation. Nat Neurosci *16,* 1499-1508. 10.1038/nn.3502

Marras, C., and Chaudhuri, K.R. (2016). Nonmotor features of Parkinson's disease subtypes. Mov Disord *31*, 1095-1102. 10.1002/mds.26510.

McGregor, M.M., and Nelson, A.B. (2019). Circuit Mechanisms of Parkinson's Disease. Neuron *101*, 1042-1056. 10.1016/j.neuron.2019.03.004.

Nagahara, A.H., and Tuszynski, M.H. (2011). Potential therapeutic uses of BDNF in neurological and psychiatric disorders. Nat Rev Drug Discov *10*, 209-219. 10.1038/nrd3366.

Palasz, E., Niewiadomski, W., Gasiorowska, A., Wysocka, A., Stepniewska, A., and Niewiadomska, G. (2019). Exercise-Induced Neuroprotection and Recovery of Motor Function in Animal Models of Parkinson's Disease. Front Neurol *10*, 1143. 10.3389/fneur.2019.01143.

Park, J., Phillips, J.W., Guo, J.Z., Martin, K.A., Hantman, A.W., and Dudman, J.T. (2002). Motor cortical output for skilled forelimb movement is selectively distributed across projection neuron classes. Sci Advances 8, eabj5167. 10.1126/sciadv.abj5167.

Park, H., and Poo, M.M. (2013). Neurotrophin regulation of neural circuit development and function. Nat Rev Neurosci *14*, 7-23. 10.1038/nrn3379.

Parker, P.R., Lalive, A.L., and Kreitzer, A.C. (2016). Pathway-Specific Remodeling of Thalamostriatal Synapses in Parkinsonian Mice. Neuron *89*, 734-740. 10.1016/j.neuron.2015.12.038.

Pasquereau, B., and Turner, R. S. (2010). Primary Motor Cortex of the Parkinsonian Monkey: Differential Effects on the Spontaneous Activity of Pyramidal Tract-Type Neurons. Cereb Ctx *21*, 1362-1378. 10.1093/cercor/bhq217

Petreanu, L., Mao, T., Sternson, S.M., and Svoboda, K. (2009). The subcellular organization of neocortical excitatory connections. Nature *457*, 1142-1145. 10.1038/nature07709

Seal, R.P., Akil, O., Yi, E., Weber, C.M., Grant, L., Yoo, J., Clause, A., Kandler, K., Noebels, J.L., Glowatzki, E., Lustig, L.R., and Edwards, R.H. (2008). Sensorineural Deafness and Seizures in Mice Lacking Vesicular Glutamate Transporter 3. Neuron *57*, 263-275. 10.1016/j.neuron.2007.11.032.

Shepherd, G.M. (2013). Corticostriatal connectivity and its role in disease. Nat Rev Neurosci *14*, 278-291. 10.1038/nrn3469

Shepherd, G.M.G., Pologruto, T.A., and Svoboda, K. (2003). Circuit analysis of experience-dependent plasticity in the developing rat barrel cortex. Neuron *38*,277-289. 10.1016/s0896-6273(03)00152-1.

Shinotsuka, T., Tanaka, Y.R., Terada, S.I., Hatano, N., and Matsuzaki, M. (2023). Layer 5 Intratelencephalic Neurons in the Motor Cortex Stably Encode Skilled Movement. J Neurosci 43,7130-7148. 10.1523/JNEUROSCI.0428-23.2023.

Smith, Y., Raju, D., Nanda, B., Pare, J.F., Galvan, A., and Wichmann, T. (2009). The thalamostriatal systems: anatomical and functional organization in normal and parkinsonian states. Brain Res Bull *78*, 60-68. 10.1016/j.brainresbull.2008.08.015.

Smith, Y., and Villalba, R. (2008). Striatal and extrastriatal dopamine in the basal ganglia: an overview of its anatomical organization in normal and Parkinsonian brains. Mov Disord *23 Suppl 3*, S534-547. 10.1002/mds.22027.

Smith, Y., Villalba, R.M., and Raju, D.V. (2009). Striatal spine plasticity in Parkinson's disease: pathological or not? Parkinsonism and Related Disorders *15S3*, S156–S161.

Stephens, B., Mueller, A.J., Shering, A.F., Hood, S.H., Taggart, P., Arbuthnott, G.W., Bell, J.E., Kilford, L., Kingsbury, A.E., Daniel, S.E., and Ingham, C.A. (2005). Evidence of a breakdown of corticostriatal connections in Parkinson's disease. Neuroscience *132*, 741754. 10.1016/j.neuroscience.2005.01.007.

Tanimura, A., Shen, W., Wokosin, D. Surmeier, D.J. (2022). Pathway-Specific Remodeling of Thalamostriatal Synapses in a Mouse Model of Parkinson's Disease. Mov Disord *37*,1164-1174. 10.1002/mds.29030.

Toy, W.A., Petzinger, G.M., Leyshon, B.J., Akopian, G.K., Walsh, J.P., Hoffman, M.V., Vuckovic, M.G., and Jakowec, M.W. (2014). Treadmill exercise reverses dendritic spine loss in direct and indirect striatal medium spiny neurons in the 1-methyl-4-phenyl-1,2,3,6tetrahydropyridine (MPTP) mouse model of Parkinson's disease. Neurobiol Dis *63*, 201209. 10.1016/j.nbd.2013.11.017.

Villalba, R.M., and Smith, Y. (2010). Striatal spine plasticity in Parkinson's disease. Front Neuroanat *4*, 133. 10.3389/fnana.2010.00133.

Villalba, R.M., and Smith, Y. (2018). Loss and remodeling of striatal dendritic spines in Parkinson's disease: from homeostasis to maladaptive plasticity? J Neural Transm (Vienna) *125*, 431-447. 10.1007/s00702-017-1735-6.

Wall, N.R., De La Parra, M., Callaway, E.M., and Kreitzer, A.C. (2013). Differential innervation of direct- and indirect-pathway striatal projection neurons. Neuron *79*, 347-60. 10.1016/j.neuron.2013.05.014

Wilson, C.J. (1987). Morphology and synaptic connections of crossed corticostriatal neurons in the rat. J Comp Neurol *263*, 567-580. 10.1002/cne.902630408

Zaja-Milatovic, S., Milatovic, D. Schantz, A.M., Zhang, J., Montine, K.S., Samii, A., Deutch, A. Y., and Montine, T. J. (2005). Dendritic Degeneration in Neostriatal Medium Spiny Neurons in Parkinson Disease. Neurology *64*, 545-547.

KEY RESOURCES TABLE

REAGENT or RESOURCE	SOURCE	IDENTIFIER
Antibodies		
Rabbit anti-tyrosine hydroxylase (1:1000, IHC)	Milipore	**RRID**: AB_390204
AffiniPure Donkey anti-rabbit Alexa Fluor 488 (1:500, IHC)	Jackson ImmunoResearch	**RRID:** AB_2313584
Streptavidin Alexa Fluor 647 (1:500, IHC)	Jackson ImmunoResearch	**RRID**: AB_2341101
Bacterial and Virus Strains		
AAV8-hSyn-DIO-hM4d(Gi)-mCherry	Addgene	**RRID**: Addgene_44362
AAV8-hSyn-DIO-mCherry	Addgene	**RRID**: Addgene_50459
Chemicals, Peptides, and Recombinant Proteins		
6-hydroxydopamine hydrochloride	Sigma Life Sciences	H4381-100mg
Cholera Toxin Subunit B, Alexa Fluor 488	ThermoFisher Scientific	C34775
Clozapine-N-Oxide	TOCRIS Bioscience	4936
SCH-23390 hydrochloride	TOCRIS Bioscience	0925
1,1'-Dioctadecyl-3,3,3',3'-Tetramethylindocarbocyanine Perchlorate (DiI)	ThermoFisher Scientific	D3911
Neurobiotin	Vector Laboratories	**RRID**: AB_2336606
AnaSed (Xylazine)	Henry Schein Animal Health	033197
Isothesia (Isoflurane)	Henry Schein Animal Health	029405
Ketoprofen (Ketofen)	Zoetis	NADA 140-269
Experimental Models: Organisms/Strains		
Slc6a3tm1(cre)Xz/J (DATcre)	Jackson Laboratories	**RRID**: IMSR_JAX:020080
B6.Cg-Tg(Drd1a-tdTomato)6Calak/J (D1dt)	Jackson Laboratories	**RRID**: IMSR_JAX:016204
Slc17a8-/- (VGLUT3-/-)	Rebecca Seal	n/a

C57Bl/6J	Jackson Laboratories	**RRID:** IMSR_JAX:000646
Software and Algorithms		
Motor Monitor	Kinder Scientific	16224-11
PRISM v8	GraphPad	**RRID:** SCR_002798
NIS-Elements	Nikon	**RRID:** SCR_014329
Fiji (ImageJ)	NIH	**RRID:** SCR_002285
Axon pCLAMP v10	Molecular Devices	**RRID:** SCR_011323

A dSPN
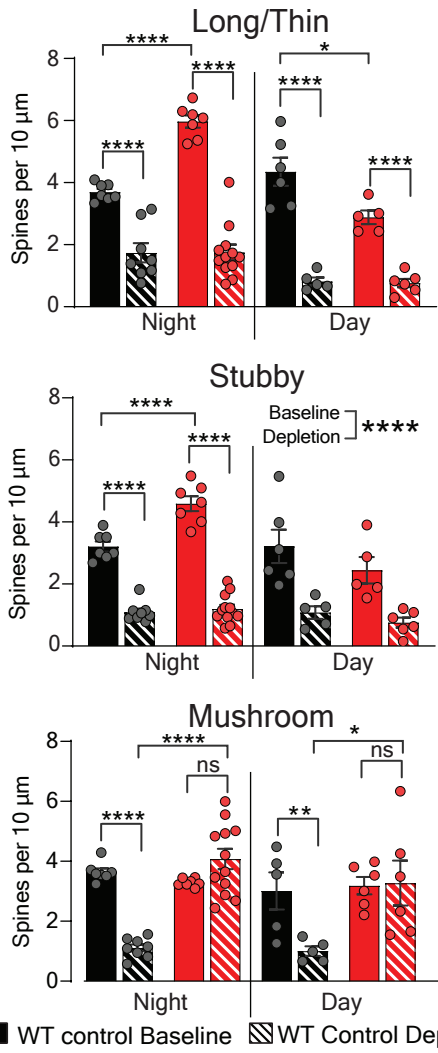
B lSPN
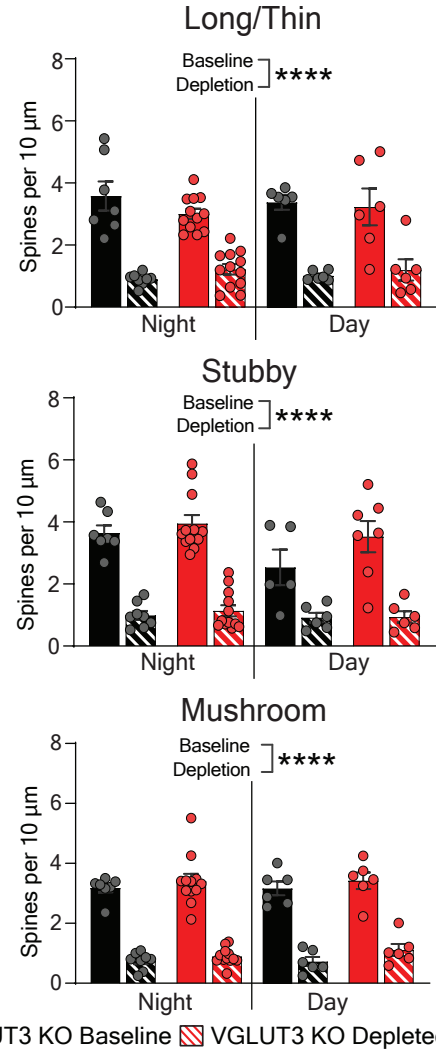
C dSPN dendrites at Night
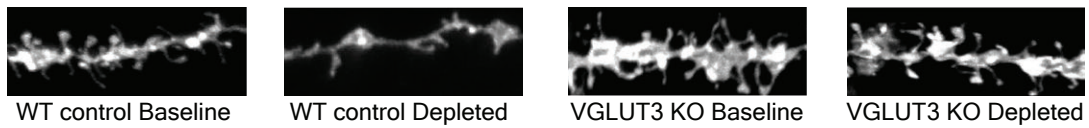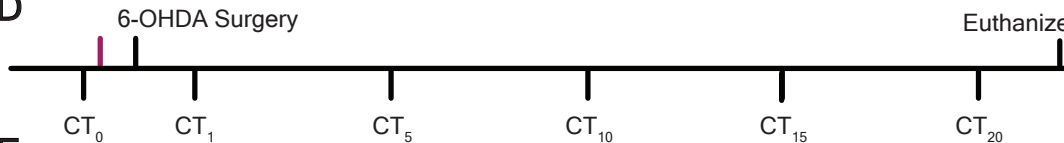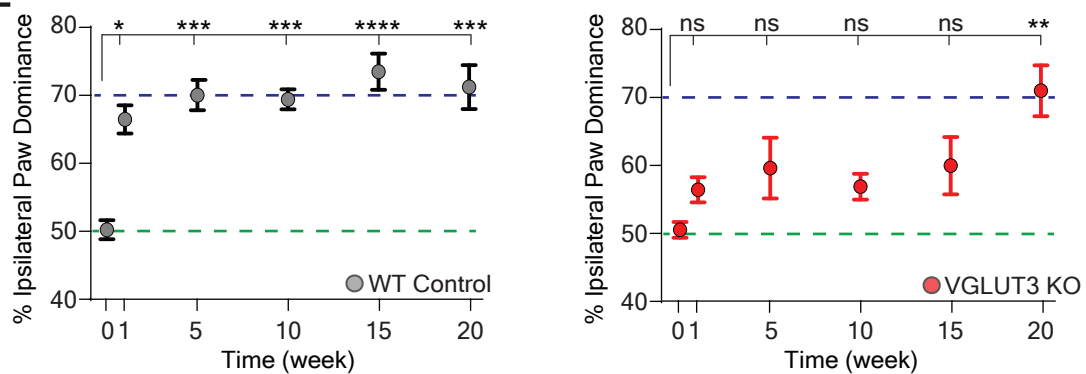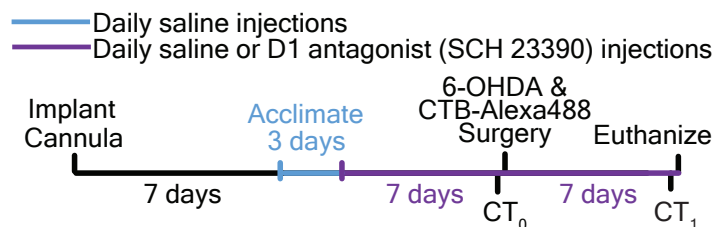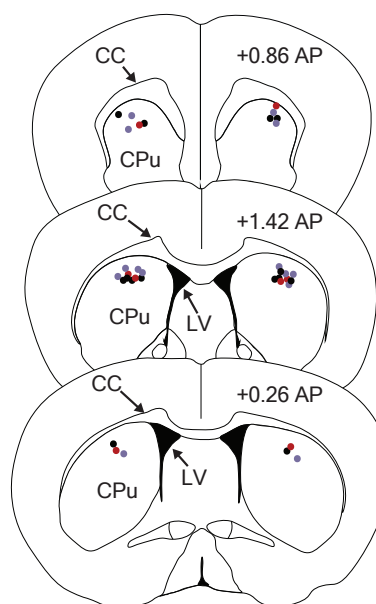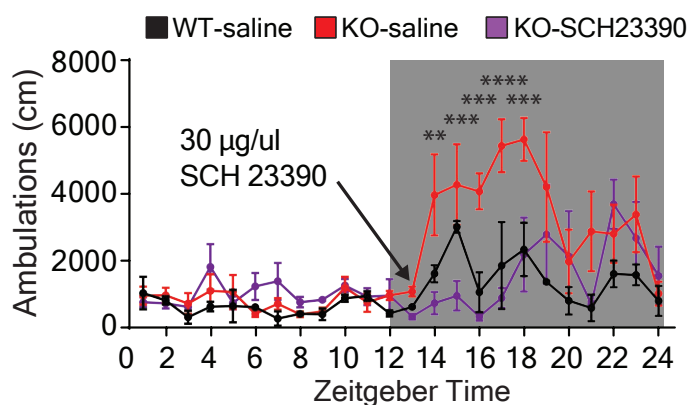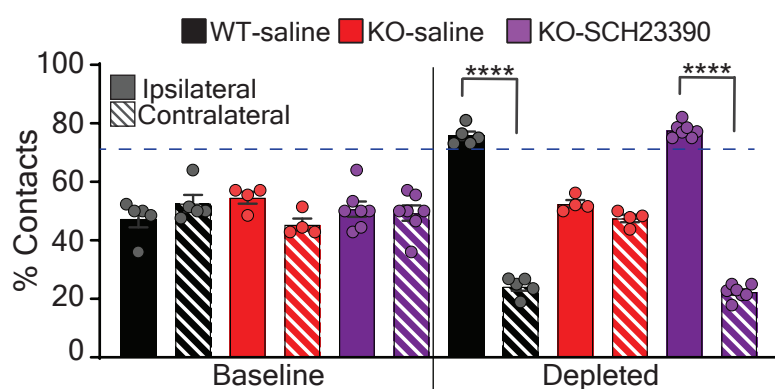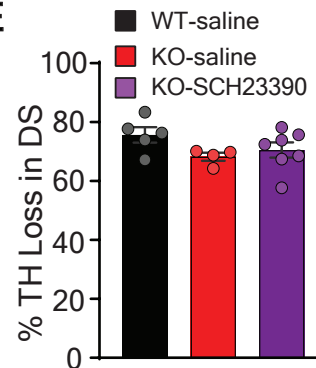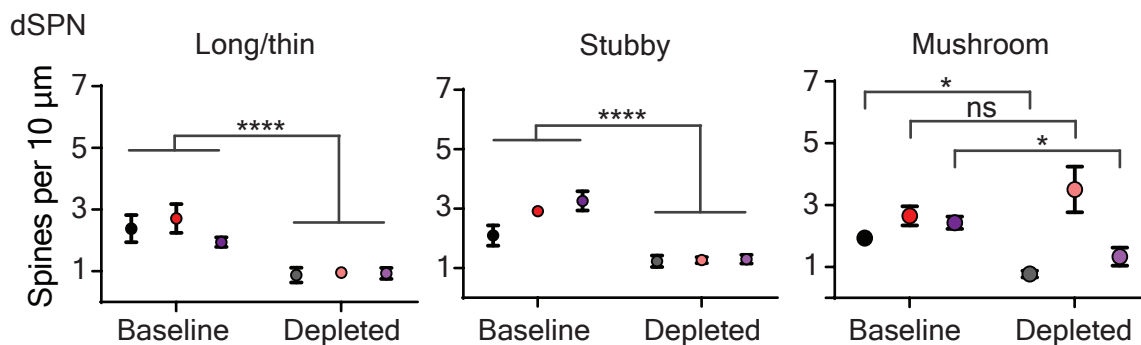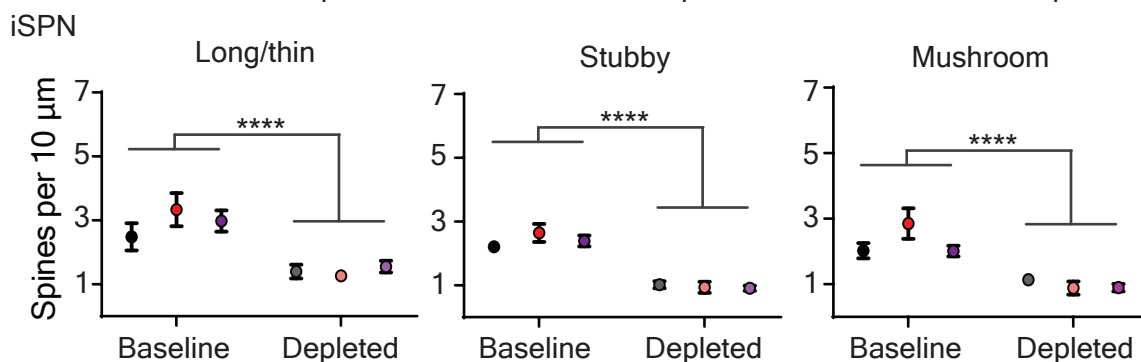
WT control Baseline   WT control Depleted   VGLUT3 KO Baseline   VGLUT3 KO Depleted
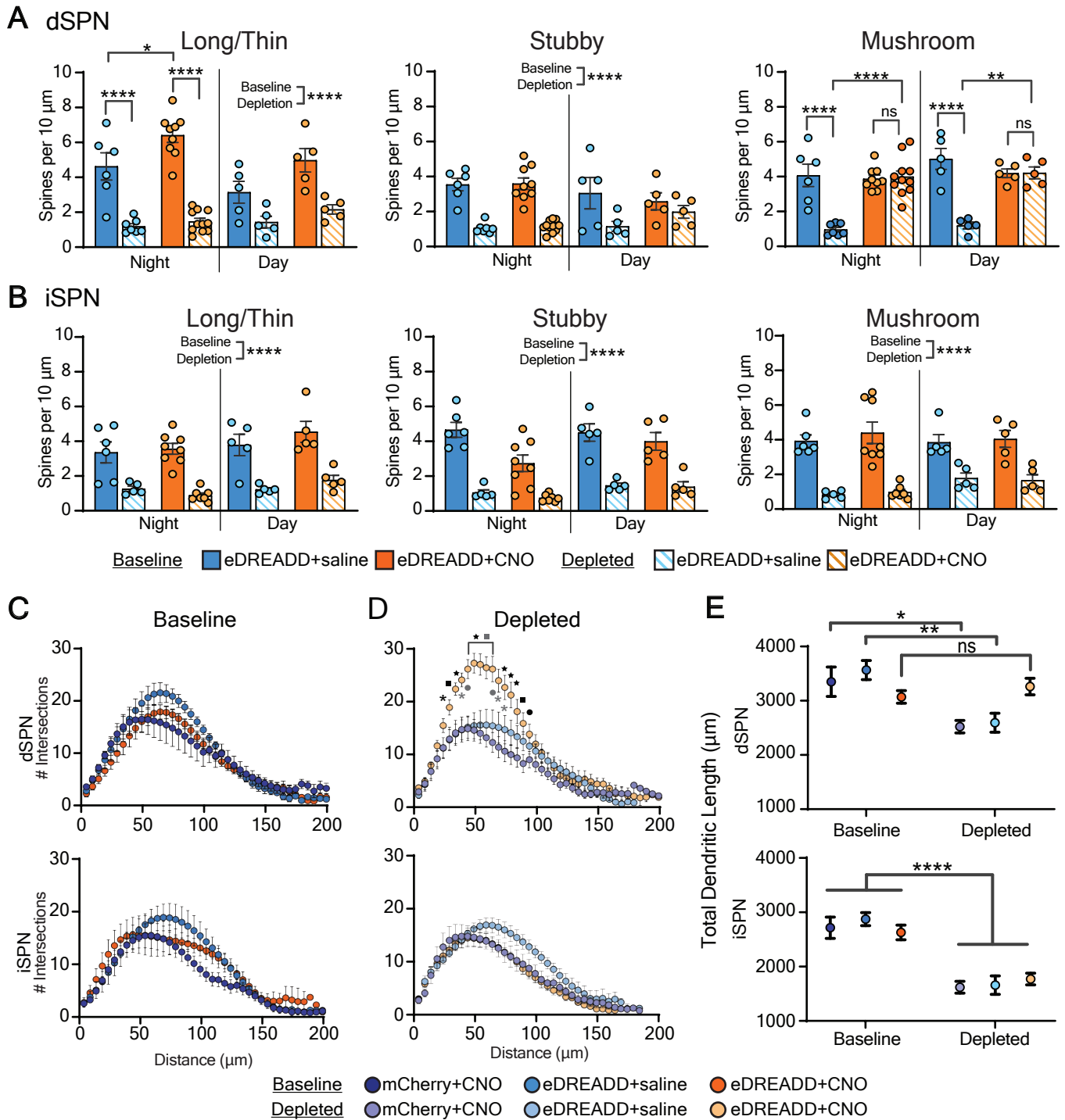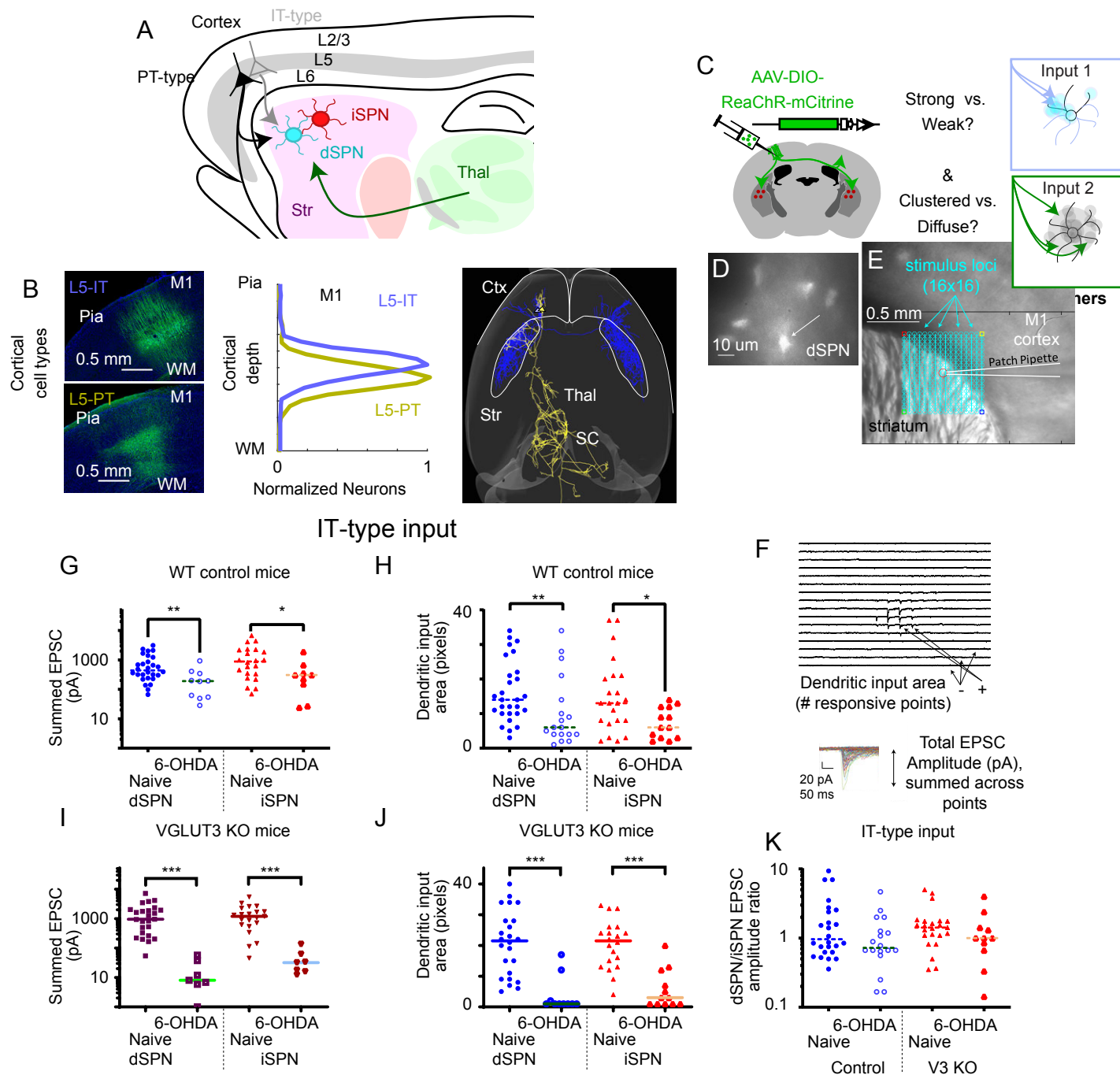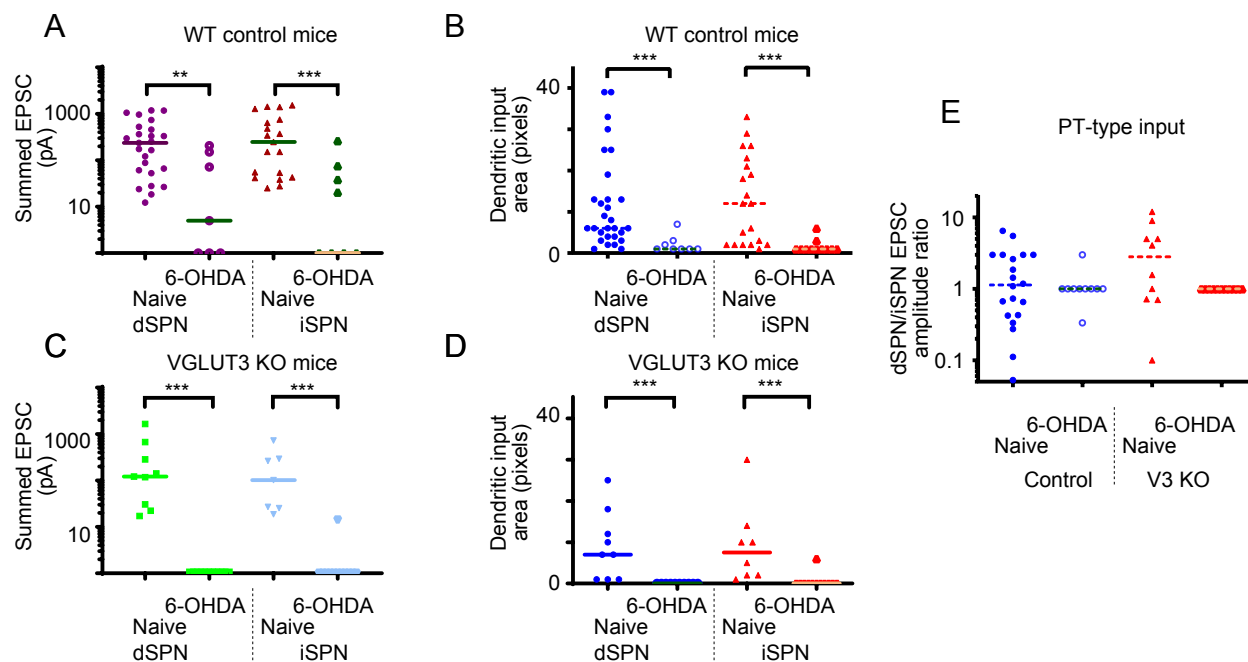
D
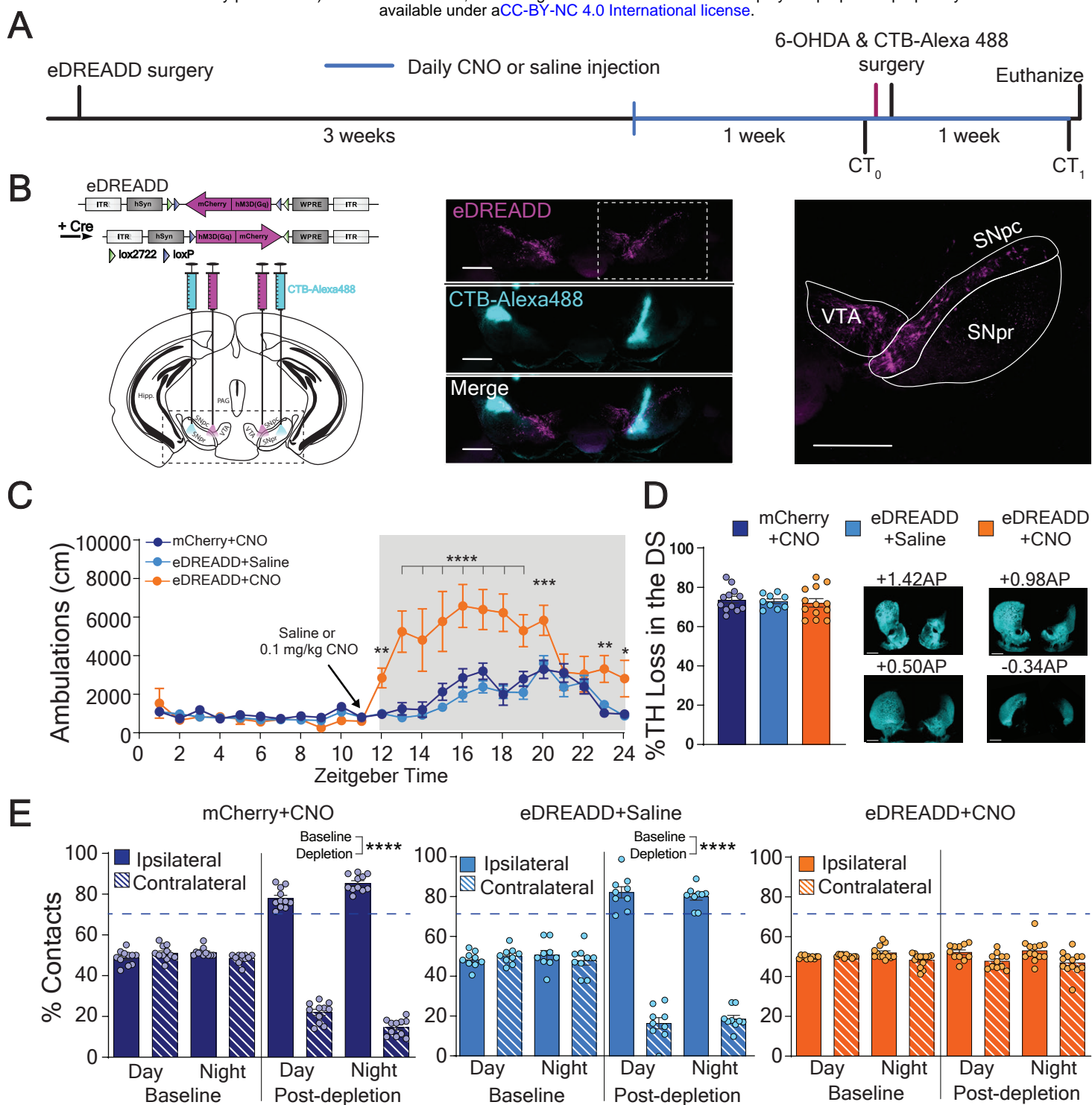
Figure 1

Figure 2

Figure 3

Figure 4

Figure 5

PT-type input

Figure 6